PERGAMON

International Journal of Heat and Mass Transfer 43 (2000) 3641–3649

International Journal of HEAT and MASS TRANSFER

www.elsevier.com/locate/ijhmt

The effect of bed diameter on near-wall hydrodynamics in scale-model circulating fluidized beds

Peter D. Noymer*, Matthew R. Hyre [1], Leon R. Glicksman

Department of Mechanical Engineering, Massachusetts Institute of Technology, Cambridge, MA 02139, USA

Received 20 April 1999; received in revised form 6 December 1999

Abstract

Previous research has shown that the diameter of a circulating fluidized bed (CFB) has a significant effect on the heat transfer rates to peripheral walls, a phenomenon important for the application of CFBs as combustors and boilers. In order to better understand the effect of bed diameter on heat transfer, two laboratory-sized scale models were built and run at room temperature. The two units were of the same height and were run at the same operating conditions with the same particles; the only difference was that the diameter of the second unit was 50% larger than that of the first. The two scale models are designed to simulate the hydrodynamic behavior in full-sized pressurized CFB combustors that are 14.3 m tall with diameters of 0.33 and 0.50 m, respectively. To compare the effect of bed diameter on hydrodynamics, the solid-fraction profiles and the fraction of the wall covered by clusters of particles were measured. The coverage of the wall by clusters was determined by analyzing images of visual data recorded with a digital high-speed video camera through the transparent bed wall. The results show that distinctly different solid-fraction profiles exist in the different-sized beds and that a 50% increase in bed diameter can nearly double the fraction of the wall covered by clusters. In addition, statistical analysis of time-resolved measurements of the wall coverage by clusters indicates that the presence of clusters follows a spatial Poisson process, i.e. the arrival of a cluster is an event that is independent from the arrival of other clusters.

1. Introduction

One issue facing designers of circulating fluidized bed (CFB) combustors is the applicability of heat transfer data from laboratory-sized scaled beds or pilot plants to full-sized commercial beds. For some early work on CFBs, there was the implicit assumption that bed-to-wall heat transfer could be correlated with respect to hydrodynamic conditions in the small bed, namely the average cross-sectional solid concentration. Recent results from larger CFBs have shown that heat transfer depends strongly on bed diameter was well as the average solid concentration [1]. This is expected since a larger-diameter bed has a lower ratio of perimeter to cross-sectional area and will accumulate more particles on the circumference for the same internal recirculation of solids per unit area in the core. Therefore, the influence of bed diameter on heat transfer is a basic phenomenon which must be understood if laboratory results are to be relevant for large-scale combustors.

* Corresponding author. Present address: Aradigm Corporation, 3929 Point Eden Way, Hayward, CA 94545, USA.

[1] Present address: Black and Decker, 123 Day Hill Road, Windsor, CT 06095, USA

0017-9310/00/$ - see front matter
PII: S0017-9310(00)00002-8

Nomenclature

c	specific heat capacity (J/kg K)
d_p	particle diameter (m)
D	bed diameter (m)
f	fraction of wall covered by clusters
g	gravitational acceleration (m/s^2)
h	heat transfer coefficient (W/m^2 K)
k	thermal conductivity (W/m K)
Nu	Nusselt number
Re_D	Reynolds number
t	cluster–wall contact time (s)
u_o	gas superficial velocity (m/s)

Greek symbols

χ^2	goodness-of-fit test parameter
δ	cluster–wall contact gap as a multiple of d_p
ε	volumetric void fraction
λ	Poisson distribution parameter
ρ	density (kg/m^3)

Subscripts

c	cluster
f	fluid
gc	gas convective
pc	particle convective
s	solid

1.1. Theory — the heat transfer model

A physical model for heat transfer to the walls of a CFB has been developed based on the cluster renewal model originally postulated for bubbling fluidized beds [2]. The CFB heat transfer model considers clusters coming to the wall from the core at the bed temperature and remaining there for a short period of time. Their contact with the heat transfer surfaces can be modeled as a transient, one-dimensional conduction process, where h_c denotes the heat transfer coefficient based on the heat flux from the cluster divided by the initial temperature difference between the wall and the cluster:

$$h_c = \sqrt{\frac{(k\rho c)_c}{\pi t}} \tag{1}$$

Furthermore, the heat transfer takes place through a small air gap between the particles and the wall, which can be modeled as a contact resistance in series with the transient conduction [3]. The total term is commonly known as "particle convective" heat transfer, or h_{pc}:

$$h_{pc} = \left(\frac{1}{h_c} + \frac{\delta d_p}{k_f}\right)^{-1} \tag{2}$$

Finally, since the wall is not completely covered by clusters of particles, the total convective heat transfer can be modeled as convection from the dilute and primarily gaseous phase acting in parallel with the convection from the dense and primarily solid phase [4]. The weighting factor is the fraction of the wall covered by clusters, or f:

$$h_{conv} = f \cdot h_{pc} + (1 - f) h_{gc} \tag{3}$$

1.2. Hydrodynamics and the heat transfer model

Several variables in the heat transfer model are governed by bed hydrodynamics and operating conditions, yet only f is clearly expected to be a function of bed diameter. Previous research has shown that ε_c is roughly a function of the average cross-sectional solid concentration and that δ is a number on the order of unity [5]. Empirical formulations for k_c show that it is a function of the gas and solid conductivities and the cluster void fraction [6], although it typically works out to be roughly twice the gas conductivity for conditions found in CFBs. t is typically expressed as a function of the falling velocity of the clusters and the contact length, but it is unclear how the either the contact length or the descent velocity will depend on bed diameter. Convection in the dilute phase can be well approximated using single-phase heat transfer correlations [5]; for turbulent, fully-developed, single-phase heat transfer in a pipe, h_{gc} is not a strong function of bed diameter ($Nu_{gc} \approx Re_D^{4/5}$, so that $h_{gc} \approx D^{-1/5}$). f is expected to vary with bed diameter as the circumferential concentration of solids changes with the ratio of perimeter to cross-sectional area. Although it is not clear if δ, ε_c, and t should depend on bed diameter, f emerges as the only heat-transfer variable that can be expected to be strongly affected by the diameter of the bed. For these reasons, our interest here lies in measuring f, as well as the average cross-sectional solid concentrations since most heat transfer data are correlated with the latter parameter.

2. Experimental apparatus

Two CFBs designed to run at room temperature were built and operated according to the same set of

specifications, except for the diameter of the beds. Both beds used the same solids material with identical mean and distribution of particle size. One bed was 50% larger than the other (51 mm versus 76 mm) while both had the same height (2.2 m) and the same abrupt 90° flow exit. The risers themselves were made of clear acrylic, thereby allowing for direct visual measurement of the flow at the wall. The operating conditions were determined based on a simplified set of scaling laws for fluidized beds [7] applied to typical CFB operating conditions. The risers were designed to be 1/6.5 scale models of the full-sized pressurized CFBs, so that the beds being simulated would be 0.33 and 0.50 m in diameter and 14.3 m tall. The superficial gas velocity for the scale models was 1.6 m/s, simulating a superficial velocity in the full-sized bed of 4.1 m/s since u_o scales with the square-root of the linear scale factor. The use of polyethylene as the solid material ($\rho_s = 910$ kg/m^3) was meant to simulate the solid-to-gas density ratio in a pressurized CFB combustor operating with a material such as limestone ($\rho_s \approx 2500$ kg/m^3) at roughly 10 atm and 1100 K. Fig. 1 shows a schematic of the CFB used in this study, and a summary of the design and operating conditions of the scale-model and hypothetical full-scale CFBs is given in Table 1.

Solid-fraction measurements were obtained at various locations along the bed from differential pressure-drop data along the wall of the riser. Observations of fractional wall coverage were made approximately 55% of the way up the bed (approximately 1.2 m above the air distributor), in a wall region 33 mm × 33 mm in the smaller bed and 50 mm × 50 mm in the larger bed. The flow of particles at the wall was recorded with a digital high-speed video system operating at an exposure rate of 250 Hz; lighting was provided by a synchronized strobe lamp. A thin (0.25 mm), black-colored plate was inserted concentrically roughly 5–10 mm from the wall in order to provide the contrast needed to identify particles in the wall region; this distance from the wall was selected to have a minimal effect on the flow of the clusters based on the observations prior to experimentation. The regions defined by the plate were roughly 11 cm^2 in the smaller bed and 25 cm^2 in the larger bed. Fig. 2 shows a schematic of the CFB riser with the black plate and strobe/camera setup. Post-processing of the digital video images with an image-analysis software package allowed for measurements of cluster size and determination of the fraction of the wall covered by clusters. Some level of judgment was required to enable the software package to define clusters.

Table 1
CFB specifications

	Models (small/large)	Full-scale (small/large)
Cross-section shape	Circular	Circular
Diameter	51/76 mm	0.33/0.50 m
Height	2.2 m	14.3 m
Gas velocity	1.6 m/s	4.1 m/s
Mean particle diameter	120 μm	≈ 240 μm
Particle sphericity	0.85	0.85
Mininum fluid velocity	0.97 cm/s	2.5 cm/s
Solid specific gravity	0.91	≈ 2.5
Bed pressure	≈ 1 atm	≈ 10 atm
Bed temperature	≈ 300 K	≈ 1100 K

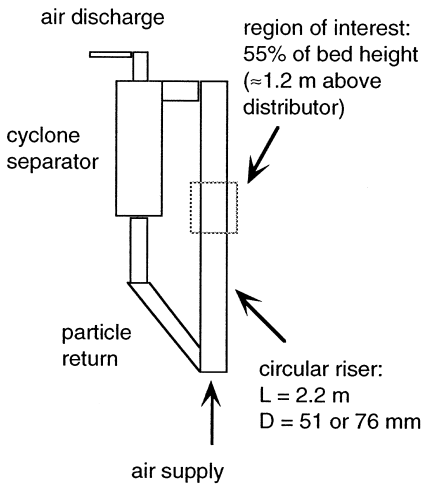

Fig. 1. Schematic of scale-model CFB.

3. Experiments and results

3.1. Experimental operating conditions

A total of six operating conditions were run: two in

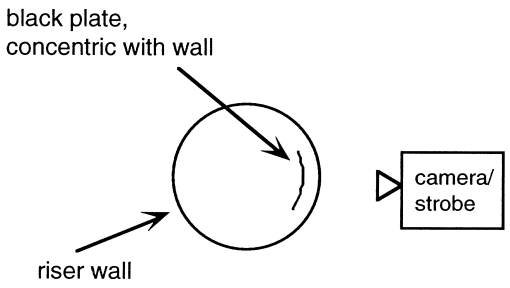

Fig. 2. Schematic of measurement region (top view).

Table 2
CFB operating conditions

Run no.	Bed size	Solids flux (kg/m^2 s)	Solid conc. @ 55% bed height
1	Large	30	1.8%
2	Large	18	1.3%
3	Small	(Not matched)	1.2% (matched)
4	Small	(Not matched)	1.8% (matched)
5	Small	30 (matched)	1.6% (not matched)
6	Small	18 (matched)	1.1% (not matched)

the larger bed and four in the smaller bed. Two experiments were first run in the larger bed in order to observe the behavior at the wall with both dense and lean average cross-sectional solid concentrations. Four experiments were run in the smaller bed to duplicate the dense and lean conditions by matching either the solids flux rate of the larger bed ("operating conditions") or by matching the average cross-sectional solid concentration at the viewing location ("local solid fraction"); matching of the local solid fraction was achieved by varying the solid recirculation rate while keeping the superficial gas velocity constant. Both matching methods were chosen in order to better understand the parameters of interest; Table 2 summarizes the conditions for each run.

3.2. Solid-fraction profiles

Because of the difference in bed diameter, matching the operating conditions did not guarantee that the average solid fraction at a given cross-sectional location would be the same. In fact, the smaller-diameter bed has a higher value of the Froude number (u_o^2/gD — which can be viewed as a ratio of gas momentum to suspension weight) and will tend toward lower cross-sectional solid concentrations for a given solids flux rate. This behavior can be seen in Fig. 3(a) and (b), which present the solid-fraction profiles for the dense and lean cases, respectively. This behavior has also been reported by Arena et al. [8], and here we see that the most significant effect on the concentration is in the lower portion of the riser.

In Fig. 3(a), the denser run in the large bed (Run #1) has a higher average cross-sectional solid concentration than the similar run in the small bed for the same solids flux rate (Run #5). The same can be said for the lean cases, shown in Fig. 3(b), when comparing Run #2 to Run #6. There is little difference between the solid-fraction profiles in the small bed when running at either the same operating conditions or local solid fraction (compare Run #4 to Run #5 or Run #3 to Run #6).

Since the only significant difference in solid concentration is near the bottom of the bed, and since heat-transfer surfaces are generally in the upper portion of the bed, one might expect that there would be little difference in heat-transfer coefficients between the smaller and larger beds. Such an expectation would be based on past research, in which heat-transfer data was generally correlated only with solid concentration.

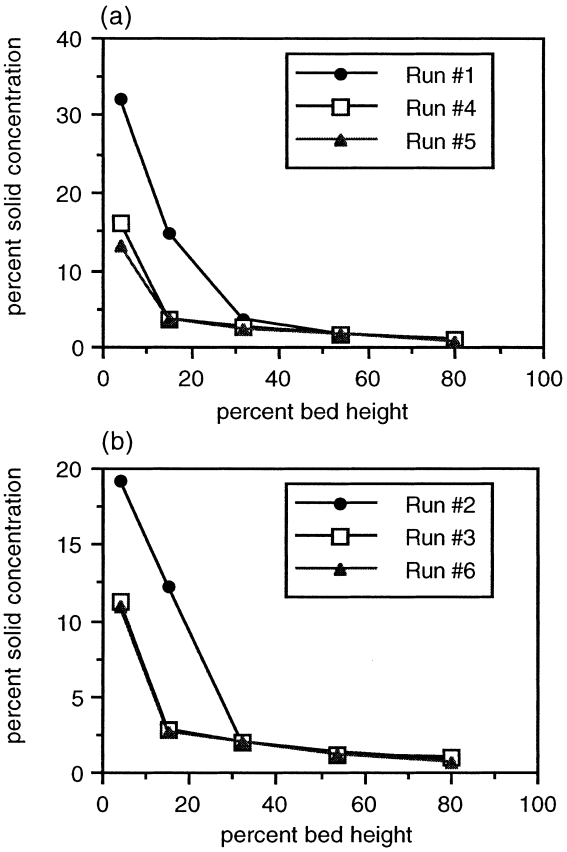

Fig. 3. Average cross-sectional solid-fraction profiles, dense cases (Run #1 — large bed; Run #4 — small bed, matched solid fraction; Run #5 — small bed, matched solids flux). (b) Average cross-sectional solid-fraction profiles, lean cases (Run #2 — large bed; Run #3 — small bed, matched solid fraction; Run #6 — small bed, matched solids flux).

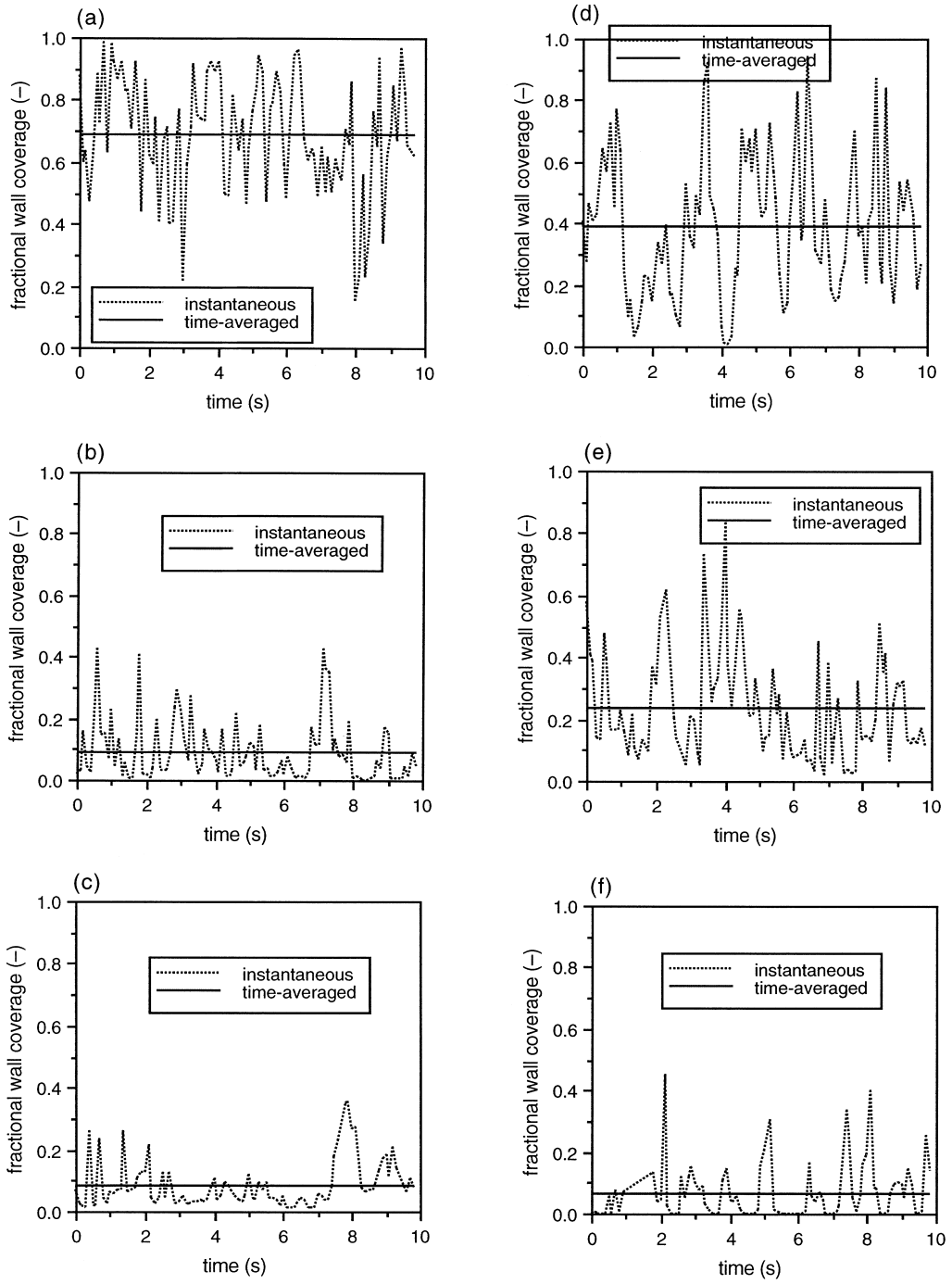

Fig. 4. Fractional wall coverage vs. time. (a) Run #1 (large bed, dense case). (b) Run #2 (large bed, lean case). (c) Run #3 (small bed, lean-matched solid fraction). (d) Run #4 (small bed, dense-matched solid fraction). (e) Run #5 (small bed, dense-matched solids flux). (f) Run #6 (small bed, lean-matched solids flux).

As mentioned previously, there appears to be an effect of the bed diameter on heat transfer, which would indicate that there are other contributors to CFB heat transfer than just solid fraction.

3.3. Fractional wall coverage

The results from these six operating conditions show that the bed with the larger diameter does indeed have a higher fraction of the wall covered by clusters. Fig. 4(a)–(f) present the measurements of instantaneous and time-averaged wall coverage for each run. Table 3 summarizes these results as the time-averaged measurements of fractional wall coverage, with separate comparisons between the large and small beds for the dense and lean cases (Run #1 versus Run #4 and Run #5, and Run #2 versus Run #3 and Run #6). As expected, the cases with the higher average cross-sectional solid concentrations show greater wall coverage (Run #4 versus Run #5, and Run #3 versus Run #6). Based on the model for heat transfer in Eq. (3), then, it appears that there may be physical explanation for increased heat transfer with bed diameter.

3.4. Fractional wall coverage — statistical analysis

Further inspection of the measurements of fractional wall coverage shows that the distribution of instantaneous measurements in each case can be best described using a Poisson distribution. Fig. 5(a)–(f) present histograms of the instantaneous measurements of fractional wall coverage for each case along with the best-fit Poisson distribution. This implies that the arrival of clusters at a given area of the wall is like a spatial Poisson process; i.e., the wall coverage can be described and characterized by a steady arrival of clusters in which each arrival event and the number of clusters arriving in each event is independent of the other events [9]. In this analysis, the Poisson distribution parameter, represented by the symbol λ, is physically equivalent to and ought to be equal to the measured fractional wall coverage. As shown in Table 4, the value of λ that best fits the data for each case is very close in value to the measured fractional wall coverage. The chi-squared (χ^2) goodness-of-fit test was used to determine the best value of λ for each case. In Table 4, we also present the ratio of the χ^2 values to the maximum allowable χ^2 values for a 95% confidence level. When this ratio is less than unity, as it is in four of the six cases, the Poisson distribution with λ for an average fractional wall coverage is appropriate [10]. In the two cases for which $\chi^2/(\chi^2)_{\max}$ exceeds unity, it does not exceed it by much, so we still retain confidence in those results.

Table 3
Experimental results

Run no.	Bed size	Matched condition	Average wall coverage
Dense cases			
1	Large	–	69%
4	Small	Solids conc.	39%
5	Small	Solids flux	24%
Leans cases			
2	Large	–	9.1%
3	Small	Solids conc.	8.4%
6	Small	Solids flux	6.6%

It is interesting to note that in the cases for which the particle concentration was leaner (Runs #2, 3 and 6), the trend of increasing f with D is not as pronounced; in fact, based on the statistical analysis, there appears to be a dependence only on average cross-sectional solid concentration. Runs #2 and 3 are the ones for which the local solid fractions were matched and they have roughly the same f or λ, while Run #6, which has a slightly lower average cross-sectional solid concentration (but the same solids flux rate as Run #2), has a slightly lower value for f or λ. The apparently different trend in f versus D for the leaner cases may be indicative of a different mechanism governing the wall coverage under lean conditions.

3.5. Fractional wall coverage — sensitivity analysis

One element of variability in the treatment of this data is the human judgement that is necessary to "teach" the image analysis software how to recognize clusters. With white particles on a black background, a "density threshold" can be set for a particular gray-scale value in regions on the image (with 256 gray-scale levels, values range from 0 for black to 255 for white). Above this density threshold, particles are close enough together to be defined as a cluster; below this density threshold, the space is either empty or the particle concentration is dilute enough so as not to contribute to the particle-convective heat transfer. Setting the proper density threshold requires sampling some of the images to see which threshold best defines the transition between the dense phase and the dilute phase of the flow. For the results presented here, the density threshold was set to a value of 30. Although this method adds uncertainty to the data, analysis of each of the cases indicates that the trends observed in the data do not change with the selected density threshold. Fig. 6(a) and (b) show that even as the selected density threshold varies, the various cases compare similarly (Fig. 6(a) is for the denser cases and Fig. 6(b) is for the leaner cases). In other words, regardless of the uncertainty in this part of the analysis, the average fractional wall coverage is always greater in the larger bed for a given set of operating conditions or for a cer-

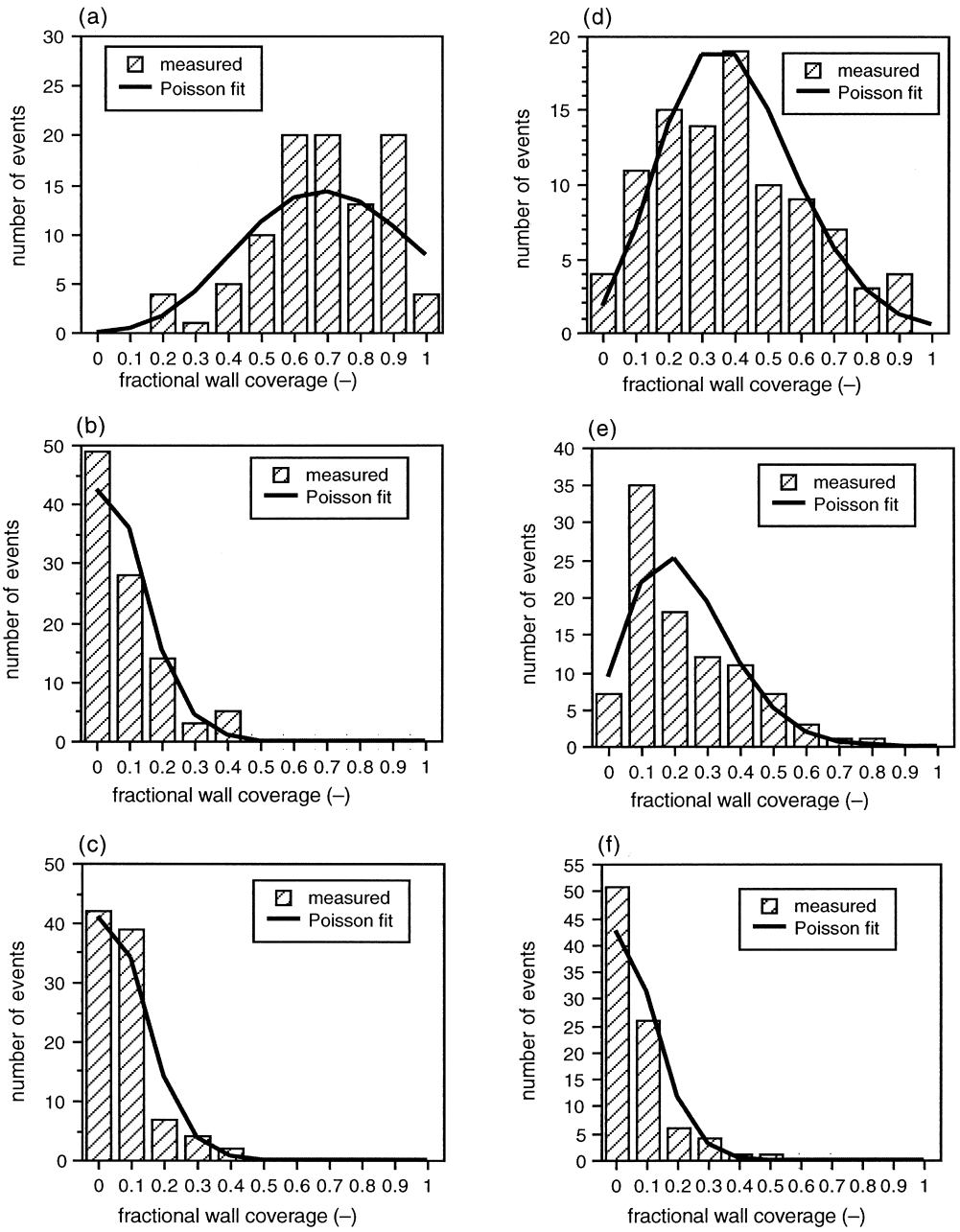

Fig. 5. Poisson fit to f measurements. (a) Run #1 (large bed, dense case). (b) Run #2 (large bed, lean case). (c) Run #3 (small bed, lean — matched solid fraction). (d) Run #4 (small bed, dense — matched solid fraction). (e) Run #5 (small bed, dense — matched solids flux). (f) Run #6 (small bed, lean — matched solids flux).

tain local solid fraction. It should be noted that Fig. 6(b) shows that a higher density threshold under lean conditions results in a slight reversal of the trend, but since the values for wall coverage are so low in those cases (less than 4%), this can be considered insignificant.

4. Conclusions

There is clearly a relationship between bed diameter and the average cross-sectional solid concentration and between bed diameter and the fractional wall coverage by clusters of particles. Between two beds in which the

Table 4
Measurements vs. statistical fits

Run no.	Bed size	Measured f (%)	Best fit λ (%)	Chi square/maximum chi square
Dense cases				
1	Large	69	73	0.89
4	Small	39	40	0.92
5	Small	24	23	1.29
Lean cases				
2	Large	9.1	8.5	0.73
3	Small	8.4	8.3	0.78
6	Small	6.6	7.4	1.15

only difference was the cross-sectional diameter, the following observations were made:

- a distinct difference exists in solid-fraction profiles, in which the larger bed is much denser in the lower portion of the riser;
- a distinct difference exists in the fraction of the wall covered by clusters, in which the larger bed has more of the bed material at the wall;
- and the coverage of the wall by clusters appears to behave like a spatial Poisson process.

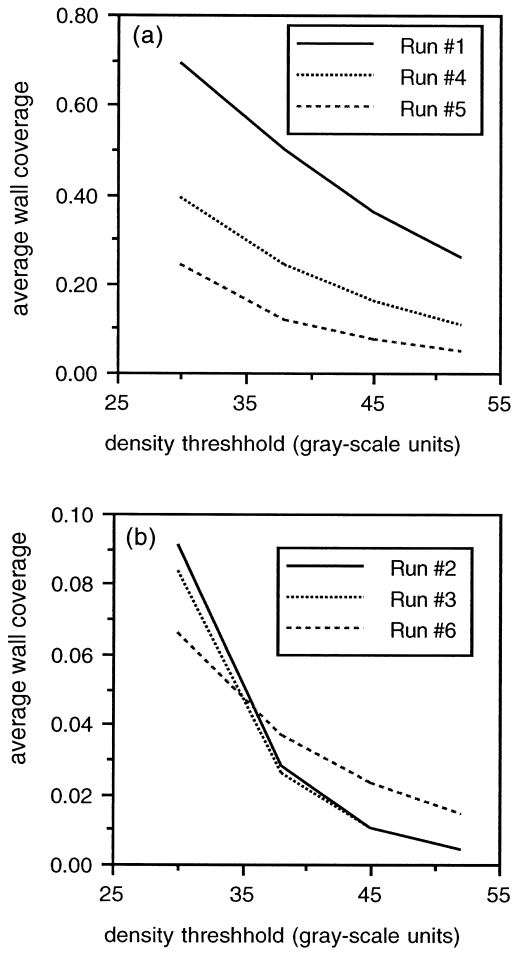

Fig. 6. (a) Sensitivity to cluster definition, dense cases. (b) Sensitivity to cluster definition, lean cases.

It should be noted that for both hydrodynamic parameters measured, especially f, there must be a limiting bed diameter beyond which no further changes are observed. Obviously, the maximum condition for wall coverage is $f = 1$, and as that limit is reached, this mechanism for increasing heat transfer must go away. Therefore, although these results are obviously applicable to the scale models that we have studied, it is unclear how they actually apply to full-sized CFB boilers that can be 10–100 times larger.

Acknowledgements

This work was sponsored by the National Science Foundation and the Electric Power Research Institute. The authors are grateful to the Edgerton Center at the Massachusetts Institute of Technology for the use of the high-speed video equipment.

References

[1] L.R. Glicksman, Heat transfer in circulating fluidized beds, in: J.R. Grace, A.A. Avidan, T.M. Knowlton (Eds.), Circulating Fluidized Beds, Chapman and Hall, London, 1997 (Chap. 8).
[2] H.S. Mickley, D.F. Fairbanks, Mechanism of heat transfer to fluidized beds, AIChE Journal 1 (1955) 374–384.
[3] A.P. Baskakov, The mechanism of heat transfer between a fluidized bed and a surface, International Chemical Engineering 4 (1964) 320–324.
[4] D. Subbarao, P. Basu, A model for heat transfer in circulating fluidized beds, International Journal of Heat and Mass Transfer 29 (1986) 487–489.

[5] M.C. Lints, L.R. Glicksman, Parameters governing particle-to-wall heat transfer in a circulating fluidized bed, in: A. Avidan (Ed.), Circulating Fluidized Bed Technology IV, AIChE, 1993, pp. 297–304.
[6] N.I. Gelperin, V.G. Einstein, Heat transfer in fluidized beds, in: J.F. Davidson, D. Harrison (Eds.), Fluidization, Academic Press, New York, 1971, pp. 471–540.
[7] L.R. Glicksman, M. Hyre, K. Woloshun, Simplified scaling relationships for fluidized beds, Powder Technology 77 (1993) 177–199.
[8] U. Arena, A. Cammarota, L. Massimilla, D. Pirozzi, The hydrodynamic behavior of two circulating fluidized bed units of different sizes, in: P. Basu, J.F. Large (Eds.), Circulating Fluidized Bed Technology II, Pergamon Press, Oxford, 1988, pp. 223–230.
[9] W. Feller, An Introduction to Probability Theory and Its Applications, vol. 1, 3rd ed., Wiley, New York, 1968 (Chap. 6).
[10] L.L. Lapin, Probability and Statistics for Modern Engineering, Brooks/Cole, Monterey, CA, 1983 (Chap. 13).